Hindawi Publishing Corporation
Advances in Condensed Matter Physics
Volume 2015, Article ID 532745, 11 pages
http://dx.doi.org/10.1155/2015/532745

Research Article

Impact of Nanoparticles on Nematic Ordering in Square Wells

M. Slavinec, E. Klemenčič, M. Ambrožič, and M. Krašna

Faculty of Natural Sciences and Mathematics, University of Maribor, Koroska 160, 2000 Maribor, Slovenia

Correspondence should be addressed to M. Slavinec; mitja.slavinec@um.si

Received 12 November 2014; Accepted 27 January 2015

Academic Editor: Charles Rosenblatt

Nematic liquid crystalline structures within square wells are studied numerically using both Lebwohl-Lasher lattice semimicroscopic and the Landau-de Gennes mesoscopic approach. At lateral boundary wall strong planar anchoring is enforced. The cell thickness h along the z Cartesian coordinate is assumed to be smaller than the characteristic square well size R. Using semimicroscopic modelling we restrict to effectively two-dimensional systems which we study in terms of the tensor nematic order parameter. We consider impact of appropriate nanoparticles (NPs) on nematic configuration for cases where R becomes comparable to the biaxial order parameter correlation length. In this case a star-like order reconstruction biaxial profile could be formed in absence of NPs. We demonstrate existence of a rich variety of different nematic structures, including topological defects, which are enabled by presence of appropriate NPs.

1. Introduction

Confined thermotropic liquid crystals (LCs) are of constant interest for years [1–3]. Due to their softness, liquid character, optical anisotropy, and rich variety of different phases and structures, they are interesting both from applicational and fundamental perspective [1, 4, 5]. Complexity of their behavior could be greatly enhanced by doping them with various nanoparticles [6–8]. The resulting configurations are referred to as soft-nanocomposites and are promising to play key role in future nano-based technology.

Uniaxial bulk nematic phase represents the simplest LC configuration exhibiting only long range orientational ordering. It is typically reached on lowering temperature from isotropic (ordinary liquid) phase via 1st order continuous symmetry breaking phase transition [1, 9, 10]. In case of weak distortions nematic local ordering could be well described by uniaxial director field $\vec{n}$ and uniaxial order parameter S. The unit vector $\vec{n}$ determines local uniaxial direction where the states $\pm\vec{n}$ are equivalent. The order parameter S describes extent of fluctuations about $\vec{n}$. It equals zero in the isotropic phase and exhibits maximal value $S = 1$ for a rigid local alignment. In bulk nematic $\vec{n}$ is homogeneously aligned along a symmetry breaking direction and S is spatially homogeneous. In general, due to continuous symmetry breaking nature [11–13] of the isotropic-nematic phase nematic patterns could contain topological defects (TDs) in the center of which $\vec{n}$ is not uniquely defined [14–18]. Furthermore, strong local distortions within cores of defect could give rise to local biaxial ordering [15, 19, 20] which necessitates description in terms of the tensor order parameter $\mathbf{Q}$. Note that TDs are in general energetically costly. Consequently in nonchiral LCs they could be stabilized only in confined geometries or in appropriate mixtures [21, 22].

In most LC-based electrooptic applications nematic configurations are confined to regular geometries [20, 23–28]. Confinement walls break the nematic translational symmetry. In addition specific anchoring and wetting conditions at walls impose different nematic patterns, including patterns possessing TDs, with potential to display rich variety of different optic textures. Recently, several studies have focused on bistable LC devices consisting of an array of micrometer-sized wells [29, 30]. Diversity of LC states is commonly enabled by boundary condition imposed frustrations. If these frustrations are imposed on a characteristic linear scale R that is large with respect to a relevant order parameter correlation length ξ then essentially uniaxial nematic patterns are formed [31]. Consequently, local orientational order was well described in terms of $\vec{n}$. However, in cases where R and ξ are comparable essentially biaxial states also appear [24, 25]. For example, for sufficiently strong antagonistic uniaxial anchorings order reconstruction (OR) structures

[23–25, 30] appear to reconcile surface-imposed frustrations. Description of OR mechanism requires picturing of nematic ordering in terms of **Q**. Order reconstruction refers to cases where spatially conflicting ordering tendencies are resolved via exchange of **Q** eigenvalues without involving a rotation of the tensor eigen frame. Typical OR structure mediating two competing regions exhibiting contradicting positive uniaxial ordering consists of a sheet possessing negative uniaxiality lying in between. This sheet is further enclosed by two sheets possessing maximal biaxiality. This sequence of nematic configurations is required topologically [4, 14, 19, 32].

In this paper we study impact of NPs on nematic structures within a square well where boundary conditions impose planar anchoring. We show that complex OR structures could appear as positions of appropriate NPs are varied within a square well. The plan of the paper is as follows. The geometry of the problem and theoretical models is introduced in Section 2. Both lattice Lebwohl-Lasher semimicroscopic-type and mesoscopic Landau-de Gennes approaches are used. In Section 3 we present simulations which result that effectively two dimensional (2D) ordering appears in systems of our interest. We also present results obtained using mesoscopic modelling where we focus on impact of NPs on LC structures. In the last section we summarize our results.

2. Modelling

Of our interest is impact of specific nanoparticles on nematic LC configurations confined to a rectangular cavity. In our study we use both lattice-type semimicroscopic and Landau-de Gennes mesoscopic modelling. In the following we first describe geometry of our interest and afterwards both theoretical approaches.

2.1. Geometry of the Problem. We consider a nematic LC sample confined within a rectangular planar (see Figure 1) cell in the Cartesian coordinate system (x, y, z), where the corresponding unit vectors pointing along coordinate axes are labeled as $(\vec{e}_x, \vec{e}_y, \vec{e}_z)$. The confining plates are placed at $x = 0$, $x = R$, $y = 0$, $y = R$, $z = 0$, $z = h$. The lateral boundaries enforce strong homogeneous tangential anchoring along corresponding Cartesian coordinates. Therefore, the plates at $x = 0$, $x = R$ enforce orientation along $\pm\vec{e}_y$, and the plates $y = 0$, $y = R$ enforce orientation along $\pm\vec{e}_x$. On the other hand we set that the top ($z = 0$) and bottom ($z = h$) surface enforce degenerate tangential anchoring. Consequently, no orientation within a (x, y) plane is singled out.

2.2. Semimicroscopic Modelling. The 3D bulk LC spin model is represented by a rectangular cell, a lattice of $M \times N \times L$ sites. Each site is occupied by a unit vector $\vec{S}(i, j, k) \equiv \vec{S}_{ijk}$ (called briefly the *nematic spin*) representing the local nematic director, where $1 \le i \le M$, $1 \le j \le N$ and $1 \le k \le L$. In order to study the dependence of the LC structure on the cell thickness, it is convenient to take lattice dimensions $M = N > L$, and to vary L. In addition, we artificially widen the lattice to the size $(M + 2) \times (N + 2) \times (L + 2)$ in the simulations to include the desired boundary conditions. The boundary planes, $i = 0$ and $M + 1$, or $j = 0$ and $N + 1$, or $k = 0$ and $L + 1$, do not represent LC nematic director and are thus not counted in the calculation of various macroscopic parameters but are used only to fix certain spin directions.

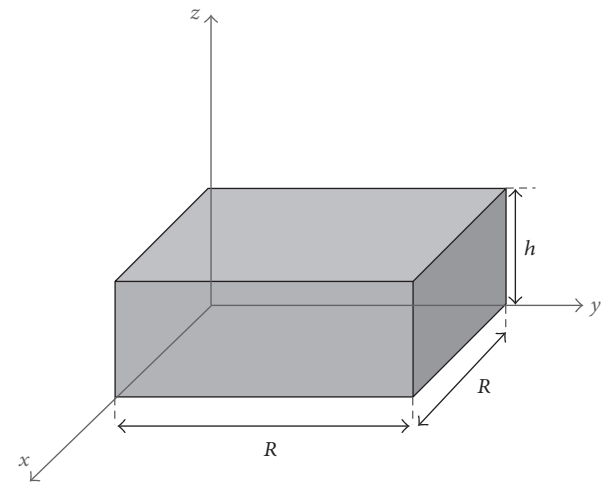

Figure 1: Nematic LC sample confined within a rectangular planar cell in the Cartesian coordinate system (x, y, z). The confining plates are placed at $x = 0$, $x = R$, $y = 0$, $y = R$, $z = 0$, $z = h$.

The strength of the interaction between the nearest nematic spins is given by positive coupling constant J. The free energy functional is modeled by the sum of the terms of all spin sites [33]:

$$F = \sum_{ijk} f_{ijk}, \tag{1}$$

where the energy term f_{ijk} consists of the sum

$$f_{ijk} = -\frac{1}{2} J \sum_{\text{n.n.}} \left(\vec{S}_{ijk} \cdot \vec{S}_{\text{n.n.}}\right)^2. \tag{2}$$

This sum represents the interactions of the nematic spin with its six nearest neighbors: the denotation $S_{\text{n.n.}}$ for the nearest neighbor thus includes $\vec{S}(i + 1, j, k)$, $\vec{S}(i - 1, j, k)$, $\vec{S}(i, j + 1, k)$, $\vec{S}(i, j - 1, k)$, $\vec{S}(i, j, k + 1)$, and $\vec{S}(i, j, k - 1)$. We must take an additional treatment of nematic spins at the simulation cell boundary. Take, for example, the spins with the first index $i = 1$. These spins lack the left neighbor spin to interact with it; they interact with the left wall corresponding to index $i = 0$, instead. Thus, in formula (2) we take the *anchoring strength* W instead of coupling constant J for the corresponding interaction. We suppose different boundary anchoring conditions for the four "side" walls ($i = 0$ or $i = M + 1$ or $j = 0$ or $j = N + 1$) as compared to "base," that is, bottom and top walls ($k = 0$ or $k = L+1$). For side walls the anchoring direction is planar horizontal; that is, $\vec{S}$ is fixed to (1, 0, 0) or (0, 1, 0), for the two pairs of opposite walls, correspondingly; the corresponding anchoring strength is denoted by W_{4s}. However, for the pair of base walls the anchoring direction is degenerate planar; that is, any direction in that plane is equivalent. This condition is considered by $\vec{S}$ being fixed to (0, 0, 1) for the two walls at $k = 0$ and $L+1$; the corresponding anchoring strength is W_{2b}. But the corresponding interaction

must be now taken with positive sign, not negative as in (2). This ensures that in order to reduce the free energy the nematic spins tend to align perpendicularly to the direction (0, 0, 1), at the base walls, that is, planar direction without any preferred easy axis.

The free energy and the three interaction magnitudes (J, W_{4s}, and W_{2b}) are next renormalized with respect to the coupling constant J by setting $J = 1$. The equilibrium spin configuration is obtained by minimizing the total free energy with respect to all the nematic spins. In order to satisfy the normalization of the spin vectors, $\vec{S}_{ijk}^2 = 1$, the "operational" total free energy must be rewritten as

$$F^* = \sum_{ijk} f_{ijk}^*, \tag{3}$$

where

$$f_{ijk}^* = \lambda_{ijk}\left(\vec{S}_{ijk}^2 - 1\right) + f_{ijk}, \tag{4}$$

with additional multiplication "constants" λ_{ijk}, which also have to be found in order to solve the system.

When thermal fluctuations of the spins have to be considered the final equilibrium state of the system is calculated through the "real-time" relaxation process including thermal disturbance. The change of spin components in the time step Δt is according to [34]

$$S_{ijk,n}\,(\text{new}) = S_{ijk,n}\,(\text{old}) + \frac{D\Delta t}{k_B T} \cdot \frac{\partial F}{\partial S_{ijk,n}}\,(\text{old}) + \Delta S^{(T)}{}_{ijk,n}, \tag{5}$$

where $S_{ijk,n}$ denotes nth component of the spin, D is the appropriate degenerated rotation diffusion tensor of the system, and k_B is the Boltzmann constant. The first term on the right side of (5) corresponds to mechanical torque which tends to rotate the spin towards equilibrium, while the second term $\Delta S^{(T)}{}_{ijk,n}$ represents random thermal fluctuation. If we introduce dimensionless time step and temperature, $\Delta t^* = Dt$, $T^* = k_B T/J$, and use (5) with dimensionless residuum vector we obtain the corresponding numerical equation:

$$\vec{S}_{ijk}\,(\text{new}) = \vec{S}_{ijk}\,(\text{old}) + 2\frac{\Delta t^*}{T^*} \cdot \vec{R}_{ijk}\,(\text{old}) + \Delta\vec{S}_T, \tag{6}$$

where we have derived the "residuum" vector quantity:

$$\vec{R}_{ijk} = \sum_{\text{n.n.}} \vec{g}\left(\vec{S}_{ijk}, \vec{S}_{\text{n.n.}}\right) \tag{7}$$

and the vector $\vec{g}$ is a function of two vectors which is defined as

$$\vec{g}\left(\vec{v}_1, \vec{v}_2\right) = \left(\vec{v}_1 \cdot \vec{v}_2\right)\left[\vec{v}_2 - \left(\vec{v}_1 \cdot \vec{v}_2\right)\vec{v}_1\right]. \tag{8}$$

The appropriate dimensionless time interval Δt^* is chosen as the input parameter according to literature: $\Delta t^* \approx 0.01$. A convenient criterion of stopping the numeric iterations is that the values of some macroscopic quantities such as free energy F or the scalar parameter S below do not change (apart from very small fluctuations) any more.

After the numeric iteration is stopped and the spins are calculated, various macroscopic quantities can be obtained. One of them is the equilibrium total energy which is conveniently normalized to one spin site:

$$\langle f \rangle = \frac{F}{MNL} \tag{9}$$

and is the average energy term per spin, $\langle S_{ijk} \rangle$ from (2).

The order of the nematic spin system can be characterized by the traceless symmetric order parameter tensor:

$$Q_{mn} = \frac{3}{2}\left\langle S_{ijk,m} S_{ijk,n} \right\rangle - \frac{1}{2}\mathbf{I}, \tag{10}$$

where $S_{ijk,m}$ is the mth component of the spin $\vec{S}_{ijk}$. The brackets $\langle \cdots \rangle$ denote the average of the quantity through the simulation cell, and $\mathbf{I}$ is the identity matrix. The eigenvalues of the $\vec{Q}_{mn}$ tensor satisfy the equation: $\lambda_1 + \lambda_2 + \lambda_3 = 0$ and are limited to the interval $(-1/2, 1)$. The scalar order parameter S is defined as the largest eigenvalue. The degree of biaxiality is measured with the *biaxiality parameter* [35]

$$\beta^2 = 1 - \frac{6\left(\text{Tr}\, Q^3\right)^2}{\left(\text{Tr}\, Q^2\right)^3} = 1 - \frac{6\left(\lambda_1{}^3 + \lambda_2{}^3 + \lambda_3{}^3\right)^2}{\left(\lambda_1{}^2 + \lambda_2{}^2 + \lambda_3{}^2\right)^3}, \tag{11}$$

where $0 \le \beta^2 \le 1$. The uniaxial states are characterized by $\beta^2 = 0$ and the states exhibiting maximal biaxiality by $\beta^2 = 1$.

2.3. Mesoscopic Modelling. We describe liquid crystalline orientational ordering using the nematic tensor order parameter [30]

$$\mathbf{Q} = \sum_{i=1}^{3} s_i \vec{e}_i \otimes \vec{e}_i, \tag{12}$$

where $\vec{e}_i$ and s_i are eigenvectors and eigenvalues of $\mathbf{Q}$, respectively. In case of uniaxial order $\mathbf{Q}$ is conventionally expressed as [1]

$$\mathbf{Q} = S\left(\vec{n} \otimes \vec{n} - \frac{1}{3}\mathbf{I}\right). \tag{13}$$

The unit vector $\vec{n}$ lies along the local uniaxial ordering direction and is referred to as the nematic director field. The scalar order parameter S expresses the magnitude of fluctuations about $\vec{n}$. Note that nematic LC ordering exhibits at mesoscopic level the so called head-to-tail invariance; that is, the orientations $\pm\vec{n}$ are equivalent.

The degree of biaxiality could be measured by the scalar parameter [35]

$$\beta^2 = 1 - \frac{6\left(\text{tr}\, \mathbf{Q}^3\right)^2}{\left(\text{tr}\, \mathbf{Q}^2\right)^3} \in [0, 1]. \tag{14}$$

Here $\beta^2 = 0$ signals uniaxial states, while an ordering with the maximum degree of biaxiality corresponds to $\beta^2 = 1$. Equality $\text{tr}\, \mathbf{Q}^3 = 3 \det \mathbf{Q}$ reveals that maximum value of β^2 is reached when at least one eigenvalue s_i vanishes.

We consider confined nematic LC and express the free energy of the system as

$$F = \int \left(f_c + f_e + f_f\right) d^3\vec{r} + \int f_s d^2\vec{r}, \tag{15}$$

where $d^3\vec{r}$ and $d^2\vec{r}$ stand for the volume and area measures, respectively. The condensation (f_c), elastic (f_e), external field (f_f) and surface (f_s) free energy densities are expressed as [30]

$$f_c = \frac{A_0\left(T - T_*\right)}{2} \operatorname{tr}\mathbf{Q}^2 - \frac{B}{3}\operatorname{tr}\mathbf{Q}^3 + \frac{C}{4}\left(\operatorname{tr}\mathbf{Q}^2\right)^2,$$
$$f_e = \frac{L}{2}\left|\nabla\mathbf{Q}\right|^2, \tag{16}$$
$$f_f = \frac{\varepsilon_0\Delta\varepsilon}{2}\vec{E}\cdot\mathbf{Q}\vec{E}.$$

Here A_0, B, and C are material constants, T stands for temperature and T_* is the supercooling temperature of the isotropic phase. The condensation term enforces $S(T < T_{\mathrm{IN}}) \equiv S_{\mathrm{eq}}(T) = (B/4C)(1 + (1 - 24A_0(T - T_*)C/B^2)^{1/2})$ and $S(T > T_{\mathrm{IN}}) = 0$. The bulk isotropic-nematic phase transition temperature is given by $T_{\mathrm{IN}} = T_* + B^2/27A_0C$. The superheating temperature of the nematic phase is realized at $T_{**} = T_* + B^2/24A_0C$. The elastic term f_e penalizing departures from a spatially homogeneous orientational ordering is weighted by a positive elastic constant L. The so called single constant approximation is used. The external field term introduces the impact of an electric field $\vec{E} = E\vec{e}$, where ε_0 stands for the electrical permittivity constant, $\Delta\varepsilon$ is the field anisotropy constant, and the unit vector $\vec{e}$ determines the orientation of the field. At the lateral surfaces we strongly impose tangential ordering. Therefore, we assume that the corresponding surface free energy density imposes strong anchoring conditions.

The important length scales [30] entering our analysis are the biaxial order parameter correlation length $\xi_b \sim \sqrt{\mathrm{LC}}/B$ and external field coherence length $\xi_f \sim \sqrt{\mathrm{LS}/(\varepsilon_0\Delta\varepsilon E^2)}$. These lengths are in general temperature dependent [30].

2.3.1. Parametrization. For a geometry given equilibrium configurations are not expected to exhibit variations along the z-axis and rotation of $\mathbf{Q}$ tensor eigen frame is restricted to (x, y) planes. A corresponding suitable order parameter tensor $\mathbf{Q}$ parametrization is given by [30, 36]

$$\mathbf{Q}(x,y) = \left(q_3 + q_1\right)\vec{e}_x\otimes\vec{e}_x + \left(q_3 - q_1\right)\vec{e}_y\otimes\vec{e}_y + q_2\left(\vec{e}_x\otimes\vec{e}_y + \vec{e}_y\otimes\vec{e}_x\right) - 2q_3\vec{e}_z\otimes\vec{e}_z, \tag{17}$$

where q_1, q_2, and q_3 are functions only of x and y. Hence, $\vec{e}_3 = \vec{e}_z$ is always an eigenvector of $\mathbf{Q}$. The remaining two eigenvectors are allowed to rotate with respect to the reference $(\vec{e}_x, \vec{e}_y)$ by an angle $\varphi \in [0, \pi)$. It holds

$$\vec{e}_1 = \cos\varphi\vec{e}_x + \sin\varphi\vec{e}_y,$$
$$\vec{e}_2 = -\sin\varphi\vec{e}_x + \cos\varphi\vec{e}_y, \tag{18}$$
$$\vec{e}_3 = \vec{e}_z.$$

The parameter q_3 reveals departures of the order parameter eigen frame $(\vec{e}_1, \vec{e}_2, \vec{e}_3)$ from the Cartesian frame $(\vec{e}_x, \vec{e}_y, \vec{e}_z)$. The two frames coincide when $q_2 = 0$. The order parameters (q_1, q_2, q_3) and eigenvalues (s_1, s_2, s_3) are related via $s_1 = q_3 + \sqrt{q_1^2 + q_2^2}$, $s_2 = q_3 - \sqrt{q_1^2 + q_2^2}$, $s_3 = -2q_3$. Note that the condition $\sqrt{q_1^2 + q_2^2} = 0$ corresponds to the exchange of eigenvalues $s_1 \leftrightarrow s_2$ in the nematic phase.

In the case of positive uniaxial ordering along $\vec{e}_1$ (i.e., $\vec{n} = \vec{e}_1$ in (13)) it holds

$$q_1 = \frac{S}{2}\cos 2\varphi, \qquad q_2 = \frac{S}{2}\sin 2\varphi, \qquad q_3 = \frac{S}{6}. \tag{19}$$

2.3.2. Scaling and Euler-Lagrange Equations. We use the scaling introduced in [35, 37], where dimensionless temperature is defined as $t = (T - T_*)/(T_{**} - T_*)$. Therefore, $t(T = T_*) = 0$, $t(T = T_{1N}) = 8/9$, $t(T = T_{**}) = 1$. For latter convenience it is customary to introduce

$$\tau = 1 + \sqrt{1 - t}. \tag{20}$$

In this scaling the equilibrium uniaxial order parameter can be expressed as

$$S_{\mathrm{eq}} = S_{**}\tau, \tag{21}$$

where $S_{**} = B/4C = S_{\mathrm{eq}}(T_{**})$.

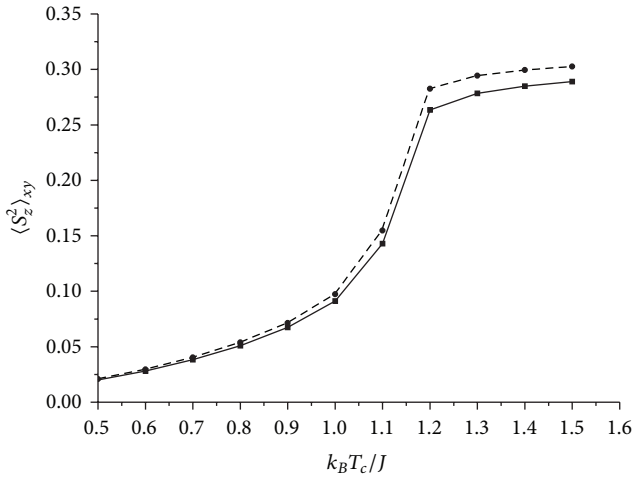

Figure 2: Temperature variation of $\langle S_z^2\rangle_{xy}$ for two different system sizes $L = R/a_0$. The isotropic-nematic phase transition takes place at $k_BT_c/J \sim 1.24$. Deep in the nematic phase the system is effectively two-dimensional. Lines are used to guide the eye.

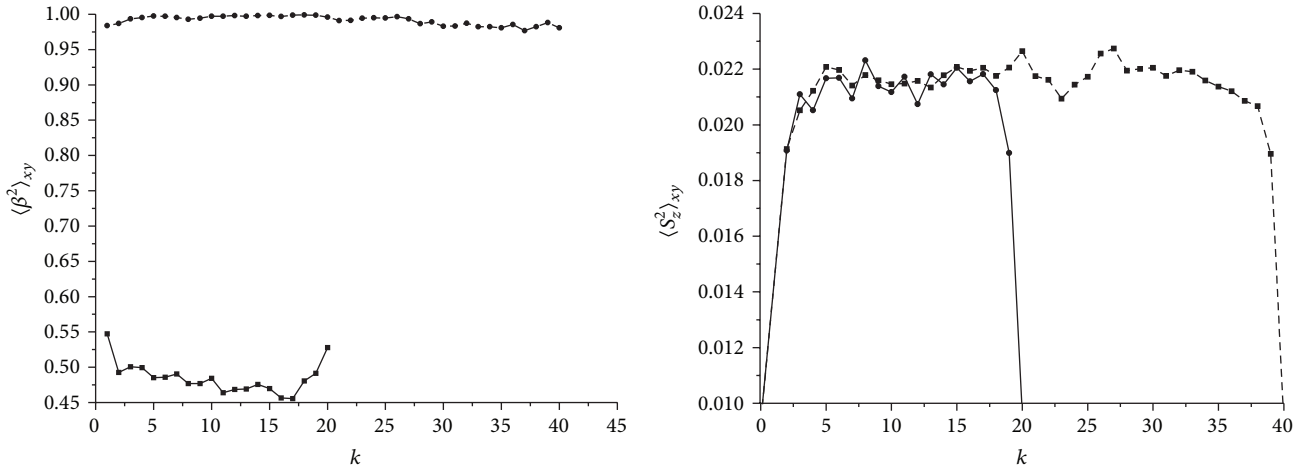

FIGURE 3: (a) Plot of $\langle\beta^2\rangle_{xy}$ as a function of $k = z/a_0$ for $L = 20$ and $L = 40$ deep in the nematic phase. (b) Plot of $\langle S_z^2\rangle_{xy}$ as a function of $k = z/a_0$ for $L = 20$ and $L = 40$ deep in the nematic phase. One sees that the nematic structure is effectively two-dimensional in the whole cell. Lines are used to guide the eye.

The key material length of systems of our interest is the biaxial correlation length. Its value is well estimated by

$$\xi_b = \frac{\xi_b^{(0)}}{\sqrt{\tau}}, \tag{22}$$

where $\xi_b^{(0)} = 2\sqrt{\mathrm{LC}}/B$ is the bare biaxial correlation length. For conventional nematics, $\xi_b \sim 20\,\mathrm{nm}$. Furthermore, we introduce the external field coherence

$$\xi_f = \sqrt{\frac{\mathrm{LS}_{**}}{\varepsilon_0 |\Delta\varepsilon| E^2}} \tag{23}$$

which is for latter convenience expressed at temperature $T = T_{**}$.

We further introduce the following scaled and dimensionless quantities: $\widetilde{\mathbf{Q}} = \mathbf{Q}/S_{**}$, $\widetilde{x} = x/R$, $\widetilde{y} = y/R$, $\widetilde{z} = z/R$, $\widetilde{\nabla} = R\nabla$, $\widetilde{F} = F/F_0$, where $F_0 = \mathrm{LS}_{**}^2 R^3/(2\xi_b^{(0)2})$. We henceforth skip the tildes bearing in mind that all quantities are scaled. The resulting dimensionless free energy F is expressed as in (15), where dimensionless free energies are given by

$$\begin{aligned} f_c &= \frac{\tau}{6}\operatorname{tr}\mathbf{Q}^2 - \frac{2}{3}\operatorname{tr}\mathbf{Q}^3 + \frac{1}{8}\left(\operatorname{tr}\mathbf{Q}^2\right)^2 \\ &= \frac{\tau}{3}\left(q_1^2 + q_2^2 + 3q_3^2\right) - 4q_3\left(q_1^2 + q_2^2 - q_3^2\right) \\ &\quad + \frac{1}{2}\left(q_1^2 + q_2^2 + 3q_3^2\right)^2, \\ f_e &= \left(\frac{\xi_b^{(0)}}{R}\right)^2 |\nabla\mathbf{Q}|^2 \\ &= 2\left(\frac{\xi_b^{(0)}}{R}\right)^2 \left(3|\nabla q_3|^2 + |\nabla q_1|^2 + |\nabla q_2|^2\right), \\ f_f &= -\frac{\Delta\varepsilon}{|\Delta\varepsilon|}\left(\frac{\xi_b^{(0)}}{\xi_f}\right)^2 \vec{e}\cdot\mathbf{Q}\vec{e} \\ &= -\frac{\Delta\varepsilon}{|\Delta\varepsilon|}\left(\frac{\xi_b^{(0)}}{\xi_f}\right)^2 \\ &\quad \cdot \Big(\left(q_3 + q_1\right)\left(\vec{e}_x\cdot\vec{e}\right)^2 + \left(q_3 - q_1\right)\left(\vec{e}_y\cdot\vec{e}\right)^2 \\ &\quad + 2q_2\left(\vec{e}_x\cdot\vec{e}\right)\left(\vec{e}_y\cdot\vec{e}\right)\Big). \end{aligned} \tag{24}$$

Minimization of the free energy yields the following bulk Euler-Lagrange equations for variational parameters q_0, q_1, and q_m:

$$\begin{aligned} &\Delta_\perp q_1\left(\frac{\xi_b^{(0)}}{R}\right)^2 - \frac{\tau}{6}q_1 + 2q_2q_1 - \frac{q_1}{2}\left(3q_2^2 + q_1^2 + q_3^2\right) \\ &\quad + \frac{1}{4}\left(\frac{\xi_b^{(0)}}{\xi_f}\right)^2 \left(\left(\vec{e}_x\cdot\vec{e}\right)^2 - \left(\vec{e}_y\cdot\vec{e}\right)^2\right) = 0, \\ &\Delta_\perp q_2\left(\frac{\xi_b^{(0)}}{R}\right)^2 - \frac{\tau}{6}q_2 + \frac{1}{3}\left(q_1^2 + q_3^2 - 3q_2^2\right) \\ &\quad - \frac{q_2}{2}\left(3q_2^2 + q_1^2 + q_3^2\right) + \frac{1}{12}\left(\frac{\xi_b^{(0)}}{\xi_f}\right)^2 = 0, \\ &\Delta_\perp q_3\left(\frac{\xi_b^{(0)}}{h}\right)^2 - \frac{\tau}{6}q_3 + 2q_2q_3 - \frac{q_3}{2}\left(3q_2^2 + q_1^2 + q_3^2\right) \\ &\quad + \frac{1}{2}\left(\frac{\xi_b^{(0)}}{\xi_f}\right)^2 \left(\vec{e}_x\cdot\vec{e}\right)\left(\vec{e}_y\cdot\vec{e}\right) = 0, \end{aligned} \tag{25}$$

where $\Delta_\perp = \partial^2/\partial x^2 + \partial^2/\partial y^2$.

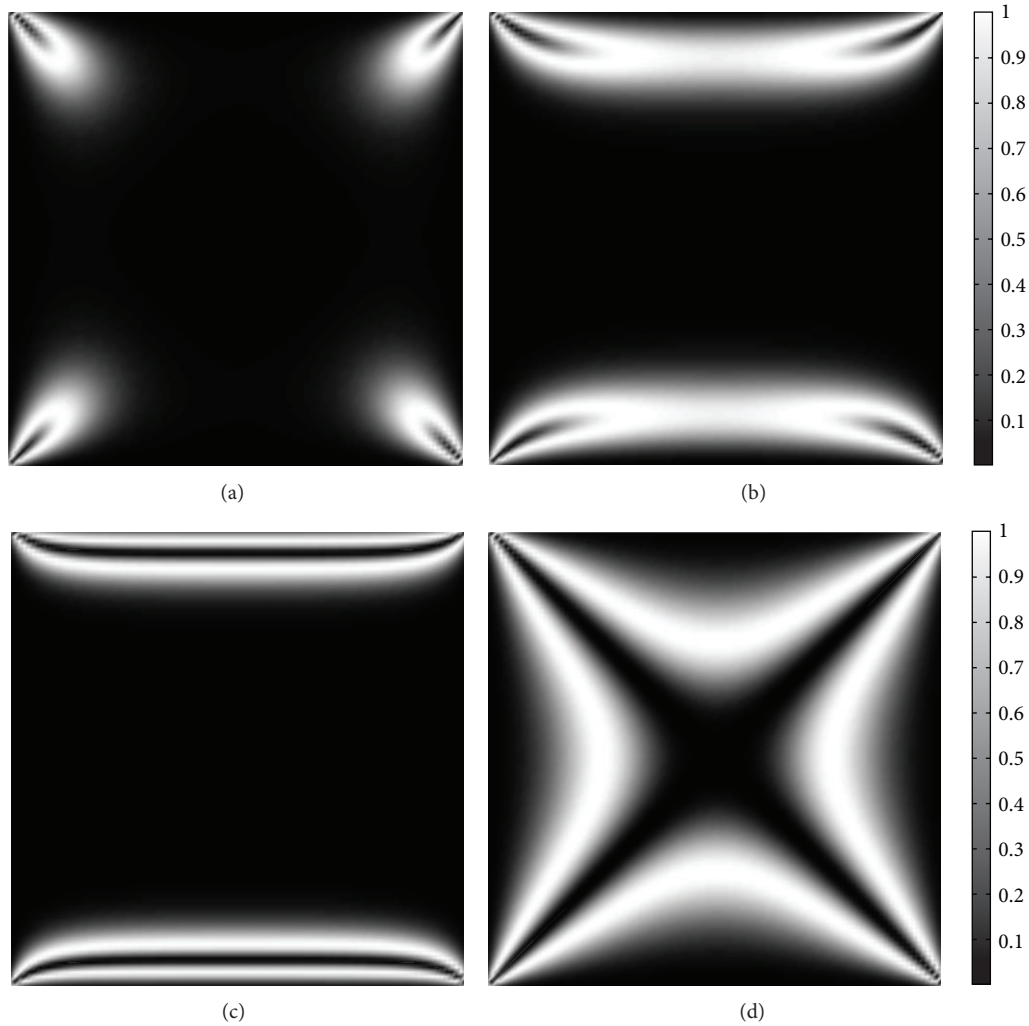

FIGURE 4: The degree of biaxiality $\beta^2(x, y)$ within a square well, $\tau = 4$, strong anchoring condition. (a) DS, $R/\xi_b = 7$, $R/\xi_f = 0$; (b) DS, $R/\xi_b = 7$, $R/\xi_f = 10$; (c) DS, $R/\xi_b = 7$, $R/\xi_f = 100$; (d) WORS, $R/\xi_b = 3$, $R/\xi_f = 0$.

3. Results

3.1. Semimicroscopic Results. In this section we analyze simulation results obtained using the lattice-type semimicroscopic approach within a cubic cell of volume R^3. In Figure 2 we plot spatial averaged squared z-component of the nematic spins $\langle S_z^2 \rangle_{xy}$ for two values of $L = R/a_0$. Here $\langle \cdots \rangle$ stands for the spatial average and a_0 stands for the lattice constant (i.e., equals separation between neighboring spins). One sees that on decreasing temperature the structure is becoming increasingly planar, that is, effectively two-dimensional. Sudden drop of $\langle S_z^2 \rangle_{xy}$ value at critical temperature corresponding to $k_B T_c/J \sim 1.24$ reveals isotropic-nematic phase transition.

In Figure 3(a) we plot $\langle \beta^2 \rangle_{xz}$ as a function of $k = z/a_0$ in the cells characterized by $L = 40$ and $L = 20$. Here $\langle \cdots \rangle_{xz}$ marks spatial averaging within the cell. Note that at the edges of surface we enforce uniaxial ordering. One sees that $\langle \beta^2 \rangle_{xz}$ relatively weakly depends on the z-coordinate spatially. Note that for large enough cells the ordering is uniaxial, corresponding to $\langle \beta^2 \rangle_{xz} = 0$. However, in our cells we see relative large value of $\langle \beta^2 \rangle_{xz}$ which increases with decreasing L. This reveals that the structures become increasingly biaxial on average for such severe confinements despite the fact that the phase transition still exists.

Finally, in Figure 3(b) we plot $\langle S_z^2 \rangle_{xy}$ as a function of $k = z/a_0$ deep in the nematic phase. One witnesses relatively small values $\langle S_z^2 \rangle_{xy}$ in the whole simulational cell. Therefore, the ordering can be considered as effectively two-dimensional for low enough temperatures.

3.2. Mesoscopic Results. In this section we analyze effectively 2D nematic structures within square wells where the lateral confinement size R is below μm and therefore comparable to the biaxial nematic order parameter correlation length ξ_b. We focus on the impact of square-shaped NPs enforcing strong planar boundary conditions on nematic configurations in absence and presence of an external electric field.

3.2.1. Absence of NPs. First, we consider cases without NPs in absence and presence of a statical ordering external field

$\vec{E} = E\vec{e}_z$. Note that the lateral walls impose strong tangential anchoring. Consequent conflicting boundary conditions at corners of a well enforce topological defects. Typical nematic structures are shown in Figures 4 and 5. In Figures 4(a) and 5 we show the so called *diagonal structure* (DS) which is stable for $R \gg \xi_b$ and $E = 0$. In most parts of the cell the nematic structure is essentially uniaxial and the nematic director field is preferentially aligned along the diagonal of the square; see Figure 5. Substantial departures from uniaxial order are surrounding defects placed at the corners of the well. Their presence is clearly seen by plotting the $\beta^2(x, y)$ spatial profile (see Figure 4(a)). For visualization purpose the structure is shown in a regime where R is comparable to ξ_b. Defects locally enforce biaxial ordering and topological characteristics of the resulting defect-core structure are known. Main defect-core features are as follows. The center of each defect exhibits negative uniaxial order along $\vec{e}_z$ and is surrounded by a rim possessing maximal degree of biaxiality $\beta^2 = 1$. Far from centers of isolated defects essentially positive uniaxial order is established in bulk. The characteristic linear size of defect-core structure is roughly determined by the biaxial length ξ_b, which reflects LC material properties at a given temperature.

On decreasing the ratio $\eta = R/\xi_b$ the so called *well order reconstruction structure* (WORS) is formed which is shown in Figure 4(d). Deep in the nematic phase this structure is stable for $\eta < \eta_c = 3.28 \pm 0.01$. In it the local eigen frames of $\mathbf{Q}$ coincide with the $\{\vec{e}_x, \vec{e}_y, \vec{e}_z\}$ laboratory frame orientation in the whole (x, y) plane. The $\beta^2 = 1$ rim exhibiting maximal biaxiality adopts an open cross-like profile. It separates regions exhibiting essentially positive uniaxial and essentially negative uniaxial ordering outside and inside the rim, respectively.

The impact of an external field for LCs with positive field anisotropy is demonstrated in Figures 4(b) and 4(c), where the field is aligned along the y-axis. The field tends to align $\vec{e}_1$ (the eigenvalue corresponding to the largest eigenvalue of $\mathbf{Q}$) along its direction. Consequently, on increasing the field strength the elastic distortions become increasingly accumulated at the top-bottom plates, because these plates enforce contradicting orientations with respect to $\vec{E}$. A typical pattern for a relatively weak field strength is shown in Figure 4(b). The top-bottom/left-right symmetry realized in absence of the field is broken. If the external field is strong enough it triggers the surface order reconstruction type of structural transition at the top-bottom plates, which is shown in Figure 4(c). We study also an alternative case where LC exhibits negative field anisotropy for the same orientation of the external field (i.e., $\vec{e} = \vec{e}_y$). In this case the field tends to orient $\vec{e}_1$ perpendicular to its direction. Consequently, the elastic distortions now accumulate at left-right plates. In both $\Delta\varepsilon > 0$ and $\Delta\varepsilon < 0$ cases the external field enforces similar biaxial textures which are rotated with respect to each other for an angle $\pi/2$ in the (x, y) plane.

3.2.2. Presence of NPs. Next, we study impact of a nanoparticle on ordering within the cell exhibiting effectively 2D behavior. Of our interest is to demonstrate existence of a rich variety of qualitatively different patterns just on varying the relative position of the nanoparticle within the cell and using different external ordering electric field $\vec{E} = E\vec{e}_y$ strengths. For this purpose we choose LC exhibiting positive field anisotropy. We choose square-shaped NP of typical length $a = R/10$. Furthermore, we set that it enforces strong tangential anchoring to surrounding LC. We place it either (1) in the center of the cell, (2) close to the left bottom well edge, or (3) close to the left boundary, and (4) close to the bottom boundary of the well. These positions of NP are schematically sketched in Figure 6. We henceforth refer to these positions as the (1) *central*, (2) *edge*, (3) *left boundary,* and (4) *bottom boundary* position.

In Figure 7 we analyze structures for $\eta = 7$ on varying E. In the first row we show cases for $E = 0$. The edges of NP are sources of elastic distortions, giving rise to locally induced

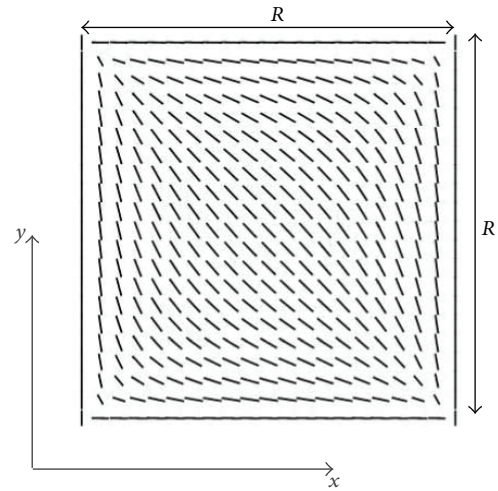

Figure 5: Orientational distribution of maximal eigenvectors of $\mathbf{Q}$ in DS. In the uniaxial limit these eigenvectors equal the nematic director field $\vec{n}$. The corresponding $\beta^2(x, y)$ dependence is plotted in Figure 4(a). $R/\xi_b = 7$, $\tau = 4$, strong anchoring condition.

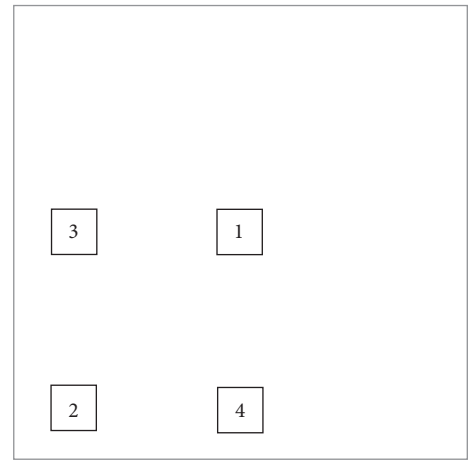

Figure 6: Schematic presentation of different positions of square-shaped NP of length $a = R/10$ within the square well. (1) *central* position, (2) *edge* position, (3) *left boundary* position, and (4) *bottom boundary* position.

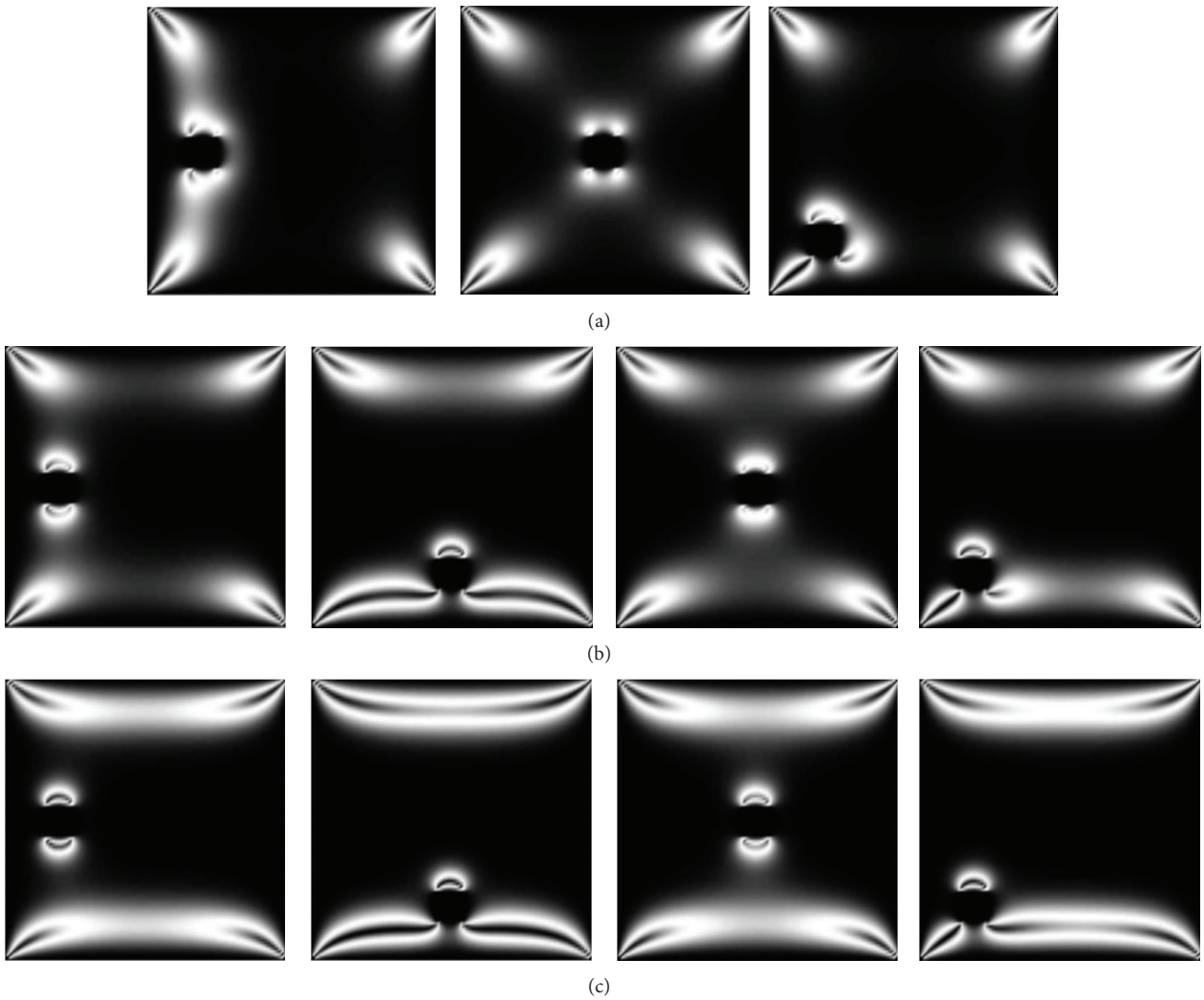

FIGURE 7: Nematic patterns for different positions of NP for $\eta = 7$. (a) $R/\xi_f = 0$. (b) $R/\xi_f = 50$. (c) $R/\xi_f = 100$.

biaxiality. We see that for all four positions of NPs the global LC structure remains qualitatively the same, although the structures are slightly different. Note that in this case patterns emerging from left boundary and bottom boundary position are the same if the patterns are rotated for $\pi/2$ about the z-axis. Next we switch on the external field of strength $R/\xi_f = 50$. Presence of the field breaks the symmetry of the problem. Its effect is increasingly pronounced for the *bottom* position of NP. In this case the mutual impact of NP and external field enables order reconstruction (OR) type transition at the bottom plate. Note that the external field alone is too weak to stabilize this type of structure. For still stronger field, that is, $R/\xi_f = 100$, we get four qualitatively different patterns. Among them the *bottom* and *edge* position support OR-type patterns.

In Figure 8 we set $\eta = 5$ which is above the threshold value $\eta_c = 3.28$ below which the WORS pattern is stable. However, we see that for the central position WORS-type pattern is nevertheless stabilized for $E = 0$ due to the presence of NP. If the external field is switched on the WORS-type pattern vanishes and is replaced by "common" OR-type structures. In this case $R/\xi_f = 50$ and $R/\xi_f = 100$ yield qualitatively similar patterns.

Finally, in Figure 9 we set $\eta = 3 < \eta_c$. For such condition the WORS pattern is stable in absence of NP. However, presence of NP does not support this pattern for the *edge* position for $E = 0$. For $R/\xi_f = 50$ and $R/\xi_f = 100$ we obtain again qualitatively similar patterns. None of them exhibits WORS-type structure.

4. Conclusions

We studied numerically combined impact of NPs and external aligning electric field on nematic structures within a square well where walls enforce planar uniaxial boundary conditions [29, 30]. Most simulations were performed at mesoscopic scale where we described nematic structures in terms of the 3D tensor order parameter **Q** [1]. We focus on regime where order reconstruction type solutions might exist. These patterns could be stabilized if a characteristic

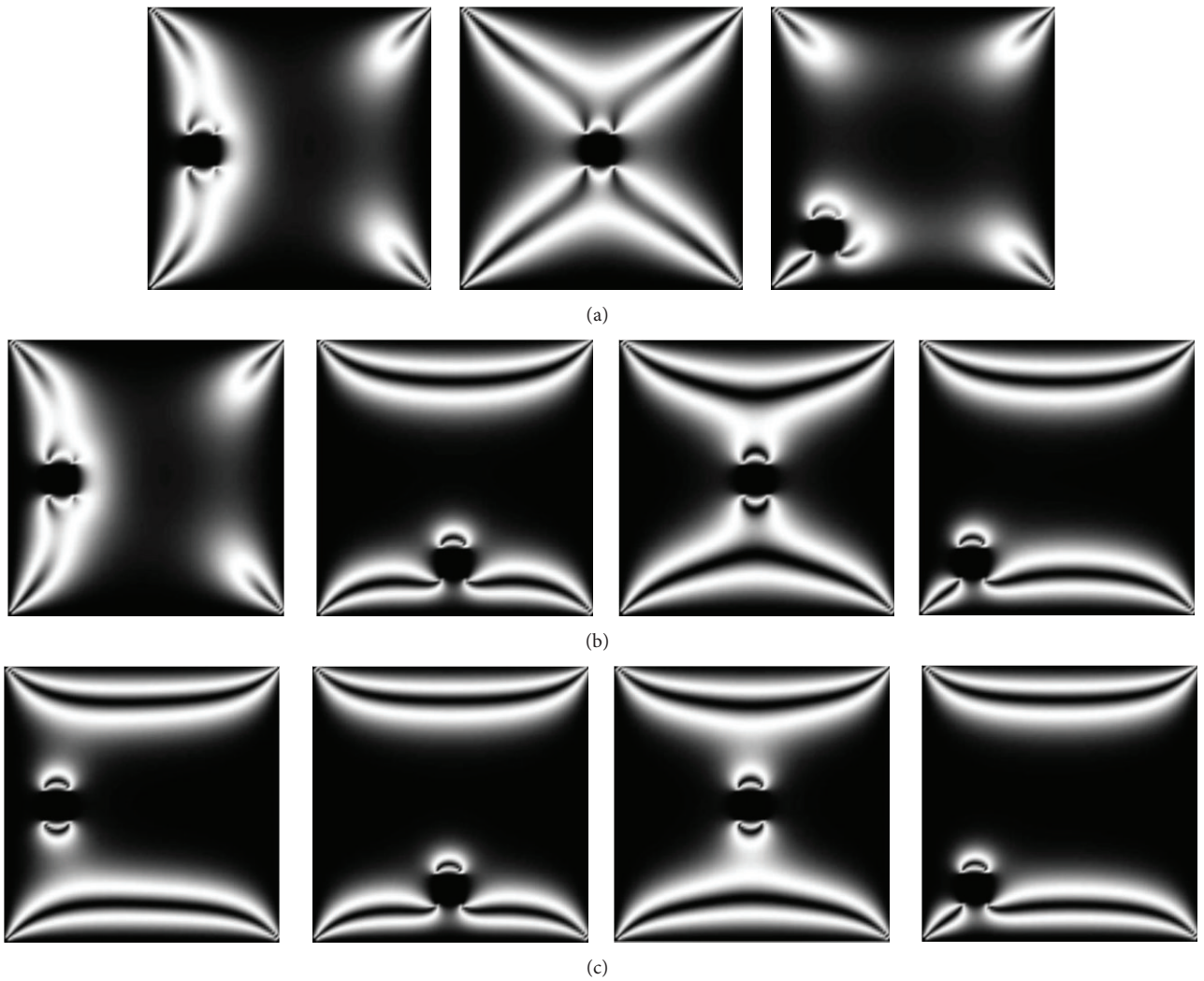

(a)

(b)

(c)

Figure 8: Nematic patterns for different positions of NP for $\eta = 5$. (a) $R/\xi_f = 0$. (b) $R/\xi_f = 50$. (c) $R/\xi_f = 100$.

lateral well size R is comparable with the biaxial order parameter correlation length ξ_b [16].

We first analyzed behavior in a 3D cubic well in absence of external field and NPs cell using a lattice-type semimicroscopic model [34]. Our simulations reveal that for given boundary conditions deep in the nematic phase LC ordering exhibits essentially 2D behavior [22]. Furthermore, results reveal that on decreasing the characteristic linear scale R of the system degree of biaxiality is apparently increasing for studied values of R. It is to be mentioned that in all cases the system size was large enough to exhibit the isotropic-nematic phase transition [34].

Based on gained knowledge in 3D semimicroscopic simulations we studied in more detail impact of NPs on structural behavior in square wells in which the height $h \ll R$, where we neglected spatial variations along the z-coordinate [29, 30]. We analyzed structures deep in the nematic phase for ratios $\eta = R/\xi_b = 7$, $\eta = 5$, and $\eta = 3$. We consider square-shaped NPs where their walls enforce strong tangential anchoring to surrounding LC. Note that in absence of external field and NPs the OR-type structure exists below the critical value $\eta_c \sim 3.28$ [30]. Our simulations show that, in particular, close to the critical value of η one could get variety of different structures just by placing the nanoparticle at different points within the well.

Note that essential features of the problem could be reproduced using 2D modelling within the (x, y) Cartesian plane using 2D tensor order parameter $\mathbf{Q}_{2D} = q_1 \vec{e}_x \otimes \vec{e}_x - q_1 \vec{e}_y \otimes \vec{e}_y + q_2(\vec{e}_x \otimes \vec{e}_y + \vec{e}_y \otimes \vec{e}_x)$. This parametrization is commonly used to study defect textures in nematic shells [22]. The relationship between commonly used 2D and our 3D parametrization can be expressed as $\mathbf{Q} = \mathbf{Q}_{2D} + \mathbf{Q}_u$, where $\mathbf{Q}_u = q_3 \vec{e}_x \otimes \vec{e}_x + q_3 \vec{e}_y \otimes \vec{e}_y - 2q_3 \vec{e}_z \otimes \vec{e}_z$ is the uniaxial tensor. Therefore, both descriptions are equivalently deep in the nematic phase for a spatially constant value of q_3. In our simulations q_3 exhibits apparent spatial variations at sites exhibiting order reconstruction changes. Therefore, the 2D and 3D approaches are expected to be different at least from quantitative point of view. Furthermore, in 2D modelling the cubic invariant is absent (i.e., $\mathrm{tr}\, \mathbf{Q}_{2D}^3 = 0$) [22]. Consequently,

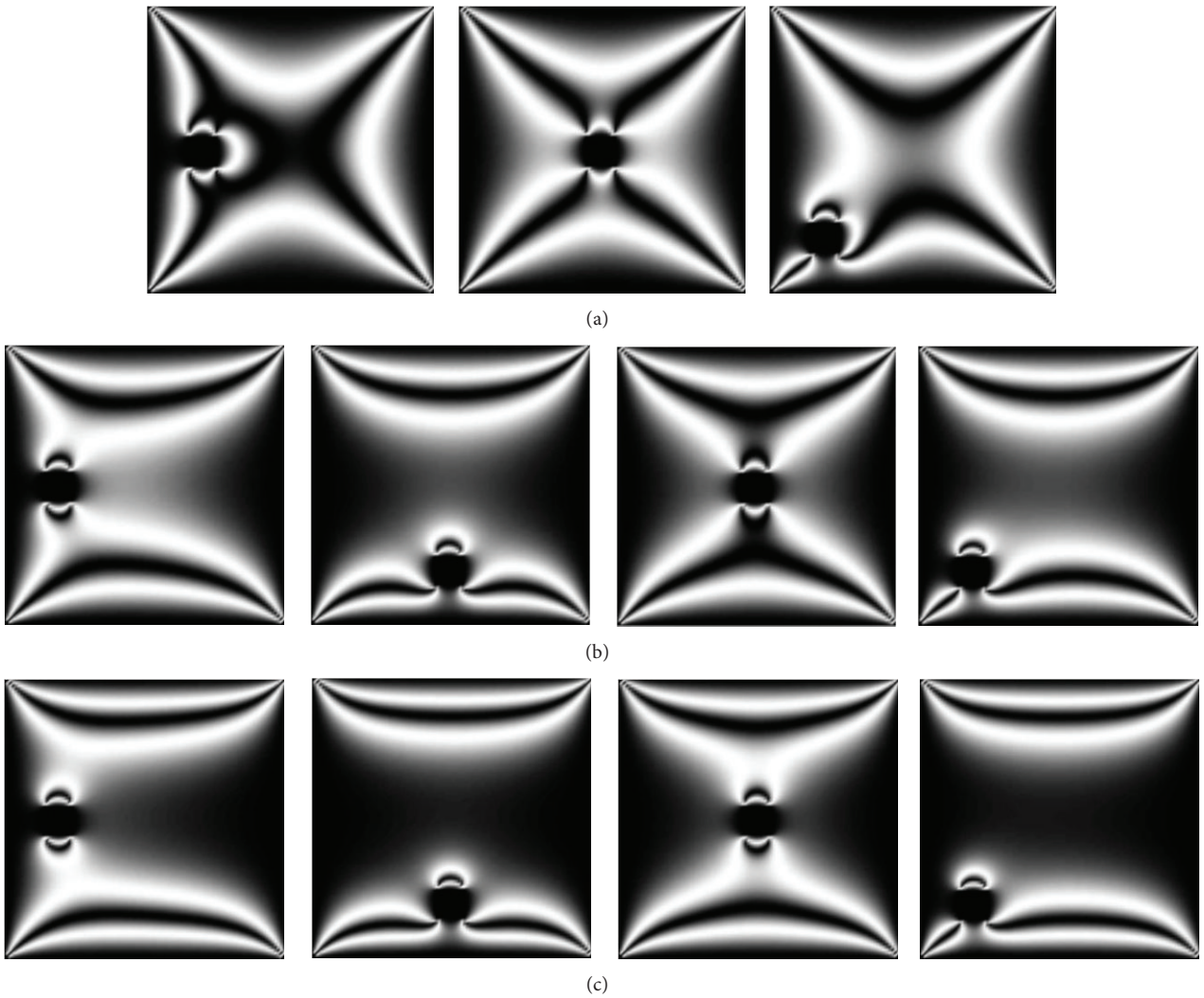

Figure 9: Nematic patterns for different positions of NP for $\eta = 3$. (a) $R/\xi_f = 0$. (b) $R/\xi_f = 50$. (c) $R/\xi_f = 100$.

using 2D modelling the *I-N* transition would be of 2nd order character. Therefore, results obtained using the 2D or 3D approach could substantially quantitatively differ close to the *I-N* phase transition.

Conflict of Interests

The authors state that there is no conflict of interests.

References

[1] M. Kleman and O. D. Lavrentovich, *Soft Matter Physics*, Springer, Berlin, Germany, 2002.

[2] Z. Kutnjak, S. Kralj, G. Lahajnar, and S. Žumer, "Calorimetric study of octylcyanobiphenyl liquid crystal confined to a controlled-pore glass," *Physical Review E*, vol. 68, no. 2, Article ID 021705, 2003.

[3] S. Tripathi, C. Rosenblatt, and F. M. Aliev, "Orientational susceptibility in porous glass near a bulk nematic-isotropic phase transition," *Physical Review Letters*, vol. 72, no. 17, Article ID 2725, 1994.

[4] G. E. Volovik and O. D. Lavrentovich, "Topological dynamics of defects: boojums in nematic drops," *Soviet Physics—JETP*, vol. 58, no. 6, pp. 1159–1166, 1983.

[5] R. Repnik, L. Mathelitsch, M. Svetec, and S. Kralj, "Physics of defects in nematic liquid crystals," *European Journal of Physics*, vol. 24, no. 4, pp. 481–492, 2003.

[6] T. Bellini, M. Buscaglia, C. Chiccoli, F. Mantegazza, P. Pasini, and C. Zannoni, "Nematics with quenched disorder: how long will it take to heal?" *Physical Review Letters*, vol. 88, no. 24, Article ID 245506, 2002.

[7] V. Popa-Nita and S. Kralj, "Liquid crystal-carbon nanotubes mixtures," *Journal of Chemical Physics*, vol. 132, no. 2, Article ID 024902, 2010.

[8] G. Cordoyiannis, V. S. Rao Jampani, S. Kralj et al., "Different modulated structures of topological defects stabilized by adaptive targeting nanoparticles," *Soft Matter*, vol. 9, no. 15, pp. 3956–3964, 2013.

[9] Z. Bradač, S. Kralj, and S. Žumer, "Molecular dynamics study of nematic structures confined to a cylindrical cavity," *Physical Review E—Statistical Physics, Plasmas, Fluids, and Related Interdisciplinary Topics*, vol. 58, no. 6, pp. 7447–7454, 1998.

[10] N. J. Mottram and C. Newton, "Introduction to Q-tensor theory," Research Report no. 10, University of Strathclyde Mathematics, Glasgow, UK, 2004.

[11] V. Popa-Nita, "Statics and kinetics at the nematic-isotropic interface in porous media," *European Physical Journal B*, vol. 12, no. 1, pp. 83–90, 1999.

[12] D. E. Feldman, "Quasi-long-range order in nematics confined in random porous media," *Physical Review Letters*, vol. 84, no. 21, pp. 4886–4889, 2000.

[13] A. Aharony and E. Pytte, "Infinite susceptibility phase in random uniaxial anisotropy magnets," *Physical Review Letters*, vol. 45, no. 19, pp. 1583–1586, 1980.

[14] O. D. Lavrentovich, "Topological defects in dispersed liquid crystals, or words and worlds around liquid crystal drops," *Liquid Crystals*, vol. 24, no. 1, pp. 117–125, 1998.

[15] N. Schopohl and T. J. Sluckin, "Defect core structure in nematic liquid crystals," *Physical Review Letters*, vol. 59, no. 22, pp. 2582–2584, 1987.

[16] M. Ambrožič, S. Kralj, and E. G. Virga, "Defect-enhanced nematic surface order reconstruction," *Physical Review E: Statistical, Nonlinear, and Soft Matter Physics*, vol. 75, no. 3, Article ID 031708, 2007.

[17] M. Svetec, S. Kralj, Z. Bradač, and S. Žumer, "Annihilation of nematic point defects: pre-collision and post-collision evolution," *European Physical Journal E*, vol. 20, no. 1, pp. 71–79, 2006.

[18] S. Kralj and T. J. Sluckin, "Core structure of a screw disclination in smectic-A liquid crystals," *Physical Review E*, vol. 48, no. 5, pp. R3244–R3247, 1993.

[19] N. D. Mermin, "The topological theory of defects in ordered media," *Reviews of Modern Physics*, vol. 51, no. 3, pp. 591–648, 1979.

[20] R. Barberi, F. Ciuchi, G. Lombardo, R. Bartolino, and G. E. Durand, "Time resolved experimental analysis of the electric field induced biaxial order reconstruction in nematics," *Physical Review Letters*, vol. 93, no. 13, Article ID 137801, 2004.

[21] S. Kralj, Z. Bradač, and V. Popa-Nita, "The influence of nanoparticles on the phase and structural ordering for nematic liquid crystals," *Journal of Physics: Condensed Matter*, vol. 20, no. 24, Article ID 244112, 2008.

[22] S. Kralj, R. Rosso, and E. G. Virga, "Curvature control of valence on nematic shells," *Soft Matter*, vol. 7, no. 2, pp. 670–683, 2011.

[23] B. Bahadur, *Liquid Crystals: Applications and Uses*, World Scientific, Singapore, 1990.

[24] G. Lombardo, H. Ayeb, and R. Barberi, "Dynamical numerical model for nematic order reconstruction," *Physical Review E*, vol. 77, no. 5, Article ID 051708, 2008.

[25] Y. Yi, G. Lombardo, N. Ashby, R. Barberi, J. E. MacLennan, and N. A. Clark, "Topographic-pattern-induced homeotropic alignment of liquid crystals," *Physical Review E—Statistical, Nonlinear, and Soft Matter Physics*, vol. 79, no. 4, Article ID 041701, 2009.

[26] P. Palffy-Muhoray, E. C. Gartland, and J. R. Kelly, "A new configurational transition in inhomogeneous nematics," *Liquid Crystals*, vol. 16, no. 4, pp. 713–718, 2006.

[27] G. Lombardo, A. Amoddeo, R. Hamdi, H. Ayeb, and R. Barberi, "Biaxial surface order dynamics in calamitic nematics," *European Physical Journal E*, vol. 35, no. 5, article 32, 2012.

[28] C. Tsakonas, A. J. Davidson, C. V. Brown, and N. J. Mottram, "Multistable alignment states in nematic liquid crystal filled wells," *Applied Physics Letters*, vol. 90, no. 11, Article ID 111913, 2007.

[29] C. Luo, A. Majumdar, and R. Erban, "Multistability in planar liquid crystal wells," *Physical Review E—Statistical, Nonlinear, and Soft Matter Physics*, vol. 85, no. 6, Article ID 061702, 2012.

[30] S. Kralj and A. Majumdar, "Order reconstruction patterns in nematic liquid crystal wells," *Proceedings of The Royal Society of London, Series A: Mathematical, Physical and Engineering Sciences*, vol. 470, no. 2169, 20140276, 18 pages, 2014.

[31] P. Palffy-Muhoray, "The diverse world of liquid crystals," *Physics Today*, vol. 60, no. 9, p. 54, 2007.

[32] A. V. Dubtsov, S. V. Pasechnik, D. V. Shmeliova, and S. Kralj, "Light and phospholipid driven structural transitions in nematic microdroplets," *Applied Physics Letters*, vol. 105, no. 15, Article ID 151606, 2014.

[33] M. Cvetko, M. Ambrožič, and S. Kralj, "Memory effects in randomly perturbed systems exhibiting continuous symmetry breaking," *Liquid Crystals*, vol. 36, no. 1, pp. 33–41, 2009.

[34] A. Ranjkesh, M. Ambrožič, S. Kralj, and T. J. Sluckin, "Computational studies of history dependence in nematic liquid crystals in random environments," *Physical Review E—Statistical, Nonlinear, and Soft Matter Physics*, vol. 89, no. 2, Article ID 022504, 2014.

[35] M. Ambrožič, F. Bisi, and E. G. Virga, "Director reorientation and order reconstruction: competing mechanisms in a nematic cell," *Continuum Mechanics and Thermodynamics*, vol. 20, no. 4, pp. 193–218, 2008.

[36] S. Kralj, R. Rosso, and E. G. Virga, "Fingered core structure of nematic boojums," *Physical Review E—Statistical, Nonlinear, and Soft Matter Physics*, vol. 78, no. 3, Article ID 031701, 2008.

[37] F. Bisi, E. C. Gartland Jr., R. Rosso, and E. G. Virga, "Order reconstruction in frustrated nematic twist cells," *Physical Review E: Statistical, Nonlinear, and Soft Matter Physics*, vol. 68, no. 2, Article ID 021707, 2003.